



Application of fluorescence probe based on NH₂-UiO-66@TAPB-PDA-COF nanocomposite in sensitive detection of carbendazim

Lei Sun^{a,b}, Rui Zhou^c, Ru-Chao Wang^b, Yue-Hong Pang^c, Xiao-Fang Shen^{c,*}

^a Xinjiang Product Quality Supervision and Inspection Research Institute (Urumqi 830011), China

^b College of Chemistry and Chemical Engineering, Xinjiang Normal University, Urumqi 830054, China

^c School of Food Science and Technology, Jiangnan University, Wuxi 214122, China

ARTICLE INFO

Keywords:

NH₂-UiO-66
TAPB-PDA-COF
Fluorescent probe
Carbendazim

ABSTRACT

Carbendazim (CBZ) residues pose serious risks to food and the environment, and the development of CBZ detection sensors is an urgent need for food and environmental monitoring. In this work, an effective and sensitive CBZ fluorescent probe based on NH₂-UiO-66@TAPB-PDA-COF was constructed using the interfacial growth method for the rapid detection of CBZ. After adding CBZ, it is adsorbed and interacts with NH₂-UiO-66@TAPB-PDA-COF through π - π interactions, hydrogen bonds, and hydrophobic interactions, resulting in electron transfer and fluorescence quenching. The fluorescence sensor has a wide concentration detection range of 1–50 μ M and shows a fast response time and a low detection limit (0.10 μ mol/L). The NH₂-UiO-66@TAPB-PDA-COF fluorescent probe has been successfully applied to the determination of CBZ residues in fruit, vegetable, water, and soil samples, with recoveries ranging from 94.21% to 107.80%. This probe method that combines MOFs with COF provides a new strategy for more rapid and accurate detection of carbendazim in food samples.

1. Introduction

Carbendazim (CBZ), an efficient and broad-spectrum benzimidazole fungicide, is widely employed in the prevention and control of fruit and vegetable diseases due to its low toxicity and strong anti-fungal activity [1,2]. Nevertheless, the global annual usage of over 80,000 tons of CBZ results in its continuous accumulation in soil and agricultural products through surface runoff and bioaccumulation. Toxicological studies have demonstrated that CBZ can induce DNA damage in human liver cells, and long-term intake may cause genetic toxicity such as chromosome telomere shortening [3,4]. Hence, the development of a highly sensitive and easy-to-operate CBZ residue detection technology is urgently required to ensure food safety and human health. The current main detection techniques, including high-performance liquid chromatography (HPLC) [5], surface enhanced Raman scattering [6], capillary electrophoresis [7] and electrochemical methods [8], encounter problems such as high instrument dependence, complex pretreatment, poor environmental adaptability, and low electrode stability in practical applications. These shortcomings make it challenging for existing technologies to meet the needs of grassroots testing institutions for rapid screening and on-site real-time detection. Therefore, it is of great significance to establish a simple, reliable, and rapid detection method for

CBZ residues in food.

In recent years, fluorescence probe technology has offered the feasibility for the rapid analysis of food safety, relying on its advantages such as rapid response, simple detection process, and visual output [9,10]. The selection of fluorescent materials is crucial to the sensitivity of fluorescence detection. Metal-organic frameworks (MOF) are porous crystal frameworks self-assembled from metal cations/clusters and organic ligands with multiple binding sites, which can enhance the adsorption capacity of target substances through ligand functionalization (such as π - π stacking, hydrophobic interaction) [11,12]. It possesses the advantages of short response time, high sensitivity, and good selectivity, and has drawn considerable attention in the field of fluorescence sensing [13,14]. Additionally, MOF has the characteristics of a large specific surface area, adjustable structure, and controllable pore size [15]. By choosing appropriate metal ions or designing organic ligands, MOF fluorescence probes with good performance can be fabricated [16]. However, because CBZ is a conjugated benzene heterocyclic compound with a logK_{ow} value of 1.49 and low polarity, the adsorption efficiency of CBZ in the hydrophilic MOF channel is insufficient, posing the problem of difficult detection. Therefore, from the perspective of material functionalization, additional functional modification of the material is carried out to further promote the adsorption of CBZ and

* Corresponding author.

E-mail address: xfshen@jiangnan.edu.cn (X.-F. Shen).

improve the detection performance.

Covalent Organic Frameworks (COFs) are crystalline porous organic polymers formed via covalent bonds, possessing excellent chemical stability and prominent specific surface area, and are extensively utilized in adsorption, sensing, separation, and other domains [17,18]. For instance, Li et al [19], fabricated a novel type of bifunctional composite material (MOFL-TPBD) through the solvothermal method. Owing to the significantly smaller radius of Pb^{2+} compared to the pore size of MOFL-TPBD, this composite material can be employed for the adsorption and separation of Pb^{2+} . Due to its innate π -conjugated system and abundant groups, it is conducive to the capture of the target. Hence, by leveraging the combination of MOF with outstanding luminescent properties and hydrophobic COFs, the conjugated electronic structure of COF and the pore channels of MOF operate synergistically, and the target object can be precisely identified through π - π stacking and hydrogen bonds [20], which is anticipated to enhance the performance of the composite material, thereby elevating the sensing performance of the sensing method.

In this study, amino-functionalized Zr-based MOFs (NH_2 -UiO-66) were utilized as carriers, and a functional nanocomposite NH_2 -UiO-66@TAPB-PDA-COF was obtained by coating TAPB-PDA-COF on the surface of NH_2 -UiO-66 via the interfacial growth method. A fluorescence probe for the rapid detection of CBZ was constructed based on this probe. By introducing the hydrophobic COF shell layer TAPB-PDA, not only the hydrophobicity of NH_2 -UiO-66 was enhanced, but also the specific surface area of the material was increased. The large π -conjugated system facilitated the enrichment of low-polarity CBZ, and the hydrophobic interface of the composite material could efficiently capture low-polarity CBZ molecules, addressing the issues of low-concentration targets and difficult access to the MOF cavity, thereby enhancing the response sensitivity of the fluorescence probe to CBZ. The application of this fluorescence probe in the detection of CBZ in actual samples was consistent with the results of high-performance liquid chromatography. This study expands the application of MOFs and COFs in the field of constructing fluorescence probes for pesticide residue sensing, providing novel ideas for pesticide residue detection.

2. Materials and methods

2.1. Materials and instruments

The materials and instruments used for the experiment are in [supporting information](#).

2.2. Synthesis of NH_2 -UiO-66@TAPB-PDA-COF

The process for preparing NH_2 -UiO-66 involves dissolving 0.105 g of $ZrCl_4$ in 30 mL of DMF, adding 0.068 g of 2-aminoterephthalic acid, and subjecting the mixture to ultrasonic treatment to achieve a uniform dispersion. Subsequently, the dispersion was transferred to a polytetrafluoroethylene reactor and reacted at 120°C for 24 h. NH_2 -UiO-66 was obtained by washing with DMF and ethanol multiple times and vacuum drying at 60°C for 12 h [21].

The process for preparing NH_2 -UiO-66@TAPB-PDA-COF entails dissolving 0.05 g of NH_2 -UiO-66 in DMSO (30 mL), vigorously stirring for 30 min, adding PDA (0.028 g) and TAPB (0.053 g), thoroughly mixing and homogenizing, adding 1 mL of acetic acid and stirring for 10 min, followed by washing with tetrahydrofuran and methanol several times and vacuum drying at 60°C for 12 h to obtain NH_2 -UiO-66@TAPB-PDA-COF [22].

2.3. Preparation of carbendazim and fluorescent probe solutions and fluorescence detection conditions

The carbendazim standard solution was prepared by weighing the carbendazim standard and making it up to 50 mL with ultrapure water to obtain a 1 mmol/L carbendazim standard solution.

The fluorescent probe solution was prepared by adding 10 mg of NH_2 -UiO-66@TAPB-PDA-COF to a 10 mL water/anhydrous ethanol (v:v = 3:1) mixed solution and diluting it to 50 μ g/mL.

In terms of the fluorescence detection conditions, the fluorescent probe without carbendazim was placed in the F-7000 fluorescence spectrometer, and the fluorescence intensity at this time was recorded as F_0 . After adding different concentrations of carbendazim standard solution, it was incubated for 5 min, and the fluorescence intensity at this time was recorded as F . In the fluorescence test process, 330 nm was selected as the excitation wavelength, with a slit width of 5 nm.

2.4. Analysis of real samples

For the exploration of the feasibility of the fluorescence probe, fruit and vegetable samples, actual water samples, and soil samples were selected for CBZ detection. Firstly, the samples were preprocessed by cutting the fruit and vegetable samples into slices and grinding them into homogeneous slurry. In the process of soil sample treatment, an appropriate amount of ultrapure water was added first, followed by ultrasound and thorough stirring using ultrasonic waves. Different volumes of CBZ standard solution were added to the fruit and vegetable samples, water samples, and soil samples respectively to maintain the concentration of CBZ in the fruit and vegetable samples, water samples, and soil. The mixed samples were filtered through a 0.22 μ m filter membrane and fluorescence detection was performed using a fluorescence probe. At the same time, high-performance liquid chromatography was used to analyze and verify this method.

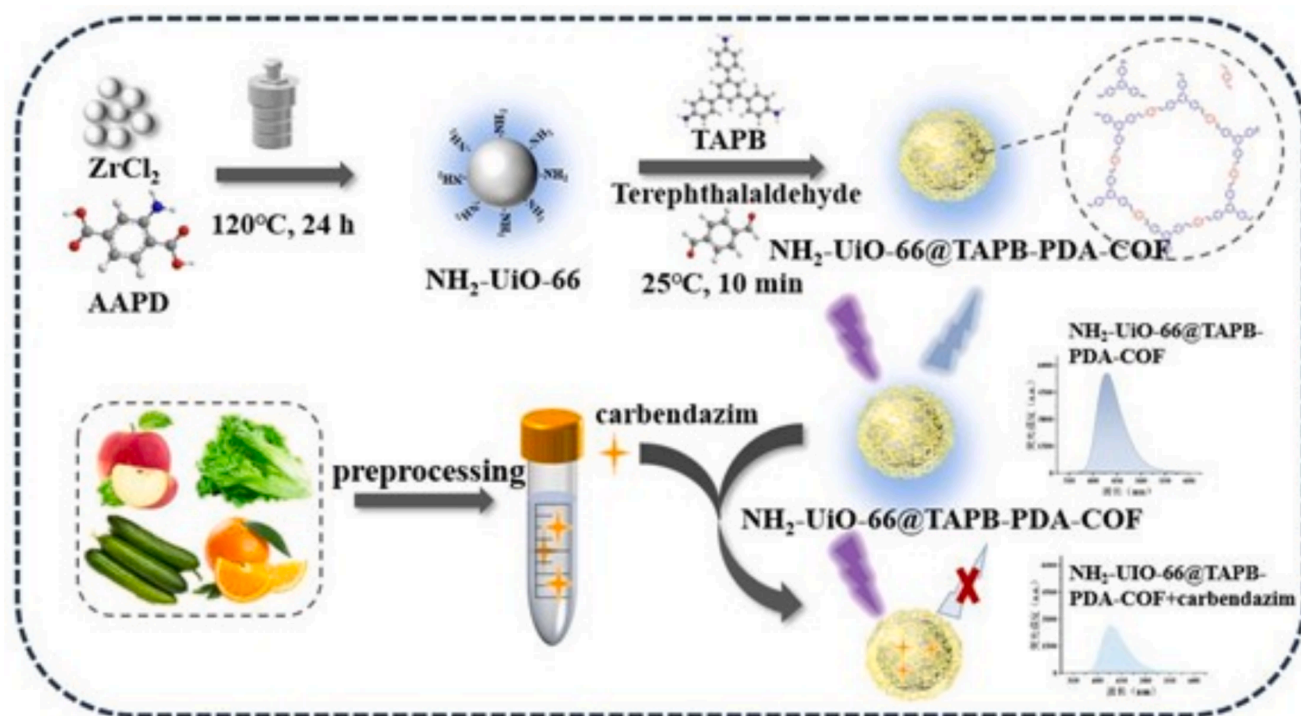
3. Results and discussion

3.1. Design and construction of fluorescent probes

Boosting the affinity between the detected substance and the detection probe is a common approach that affects the fluorescence intensity and sensitivity of fluorescent molecules. Therefore, for the detection of CBZ, the hydrophobicity and specific surface area of NH_2 -UiO-66 are increased by compounding it with TAPB-PDA-COF with a large π -conjugated system, to enhance the affinity and facilitate the enrichment of CBZ [23]. Electron transfer occurs between CBZ and the surface functional groups of the composite material through hydrogen bonds and π - π interactions, quenching the fluorescence of the composite material, enabling the rapid detection of CBZ [24]. And through HPLC, it is verified that this method can detect CBZ sensitively (Scheme. 1).

3.2. Characterization of NH_2 -UiO-66@TAPB-PDA-COF

This is the first time that the NH_2 -UiO-66@TAPB-PDA-COF composite was synthesized by modifying the surface of NH_2 -UiO-66 with TAPB-PDA-COF. NH_2 -UiO-66 exhibited a spherical morphology with aggregation through scanning electron microscopy (SEM) (Fig. 1A), consistent with the morphology described in the literature [25]. TAPB-PDA-COF showed a spherical morphology with a honeycomb-like main body (Fig. 1B). NH_2 -UiO-66@TAPB-PDA-COF had a similar solid morphology to NH_2 -UiO-66, but due to the growth of honeycomb-like TAPB-PDA-COF on the original NH_2 -UiO-66, it had a rougher surface, which was beneficial for the enrichment of CBZ on its surface (Fig. 1C). These findings proved the successful synthesis of the NH_2 -UiO-66@TAPB-PDA-COF composite. The morphological features of the nanocomposites with a typical core-shell structure can be distinctly observed through the characterization analysis by transmission electron microscopy (TEM) (Fig. 1D). The high-resolution images reveal that the TAPB-PDA-COF covalent organic framework layer attains complete coating on the surface of the NH_2 -UiO-66 metal-organic framework core via the heterogeneous nucleation mechanism, demonstrating the successful construction of the fluorescent probe of the core-shell heterostructure.



Scheme 1. Construction of NH_2 -UiO-66@TAPB-PDA-COF fluorescent sensor for CBZ detection.

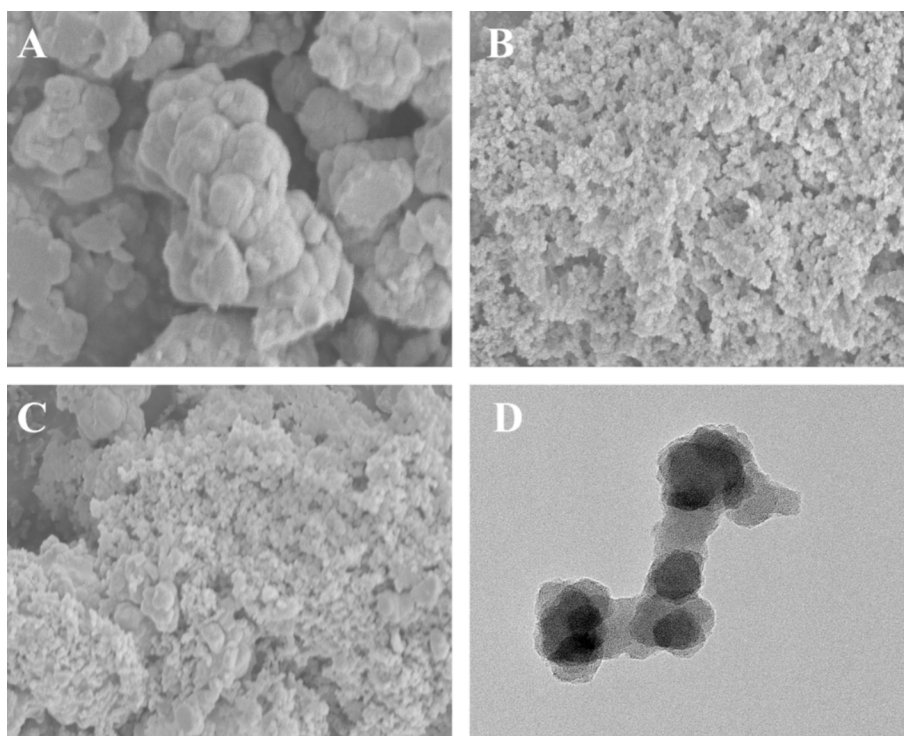


Fig. 1. SEM images of (A) NH_2 -UiO-66, (B) TAPB-PDA-COF, and (C) NH_2 -UiO-66@TAPB-PDA-COF.

The crystal structure of the material was characterised and analysed using X-ray diffraction (XRD). The experimental results show that the characteristic diffraction peaks attributed to the (111) and (002) crystal planes of NH_2 -UiO-66 at $2\theta = 7.31^\circ$ and 8.37° , respectively, confirm that the metal-organic framework material has an intact crystal lattice structure, while the covalent organic framework material of TAPB-PDA-COF exhibits its characteristic diffraction response at $2\theta = 17.45^\circ$ and

23.08° , respectively. In the XRD spectra of the materials prepared by in situ composite, the characteristic diffraction peaks of NH_2 -UiO-66 and the diffraction peaks of TAPB-PDA-COF are completely retained without new heterogeneous peaks, which indicates that the composite process effectively maintains the lattice structure of the two parent materials [26], and the structure of the heterogeneous components has been successfully achieved Composite (Fig. 2A).

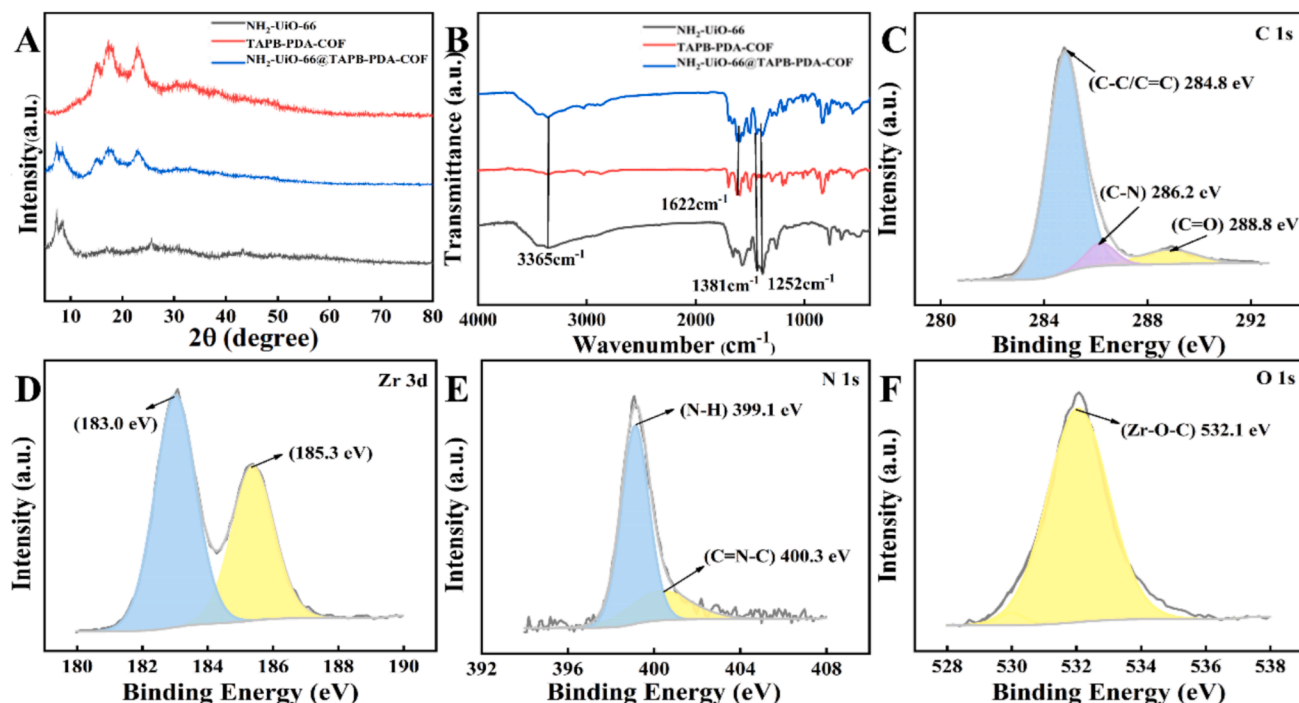


Fig. 2. (A) XRD spectra of $\text{NH}_2\text{-UiO-66}$, TAPB-PDA-COF and $\text{NH}_2\text{-UiO-66@TAPB-PDA-COF}$. (B) Fourier transform infrared (FT-IR) spectra; (C) C 1s, (D) Zr 3d, (E) N 1s and (F) O 1s high-resolution XPS spectra.

The groups present in the composite material were further analyzed using FT-IR. In the composite material, a characteristic peak was observed at 3365 cm^{-1} , which belongs to the N-H symmetric and asymmetric stretching vibrations of primary amine. The characteristic peaks at 1625 and 665 cm^{-1} belong to the C-O bending vibration and Zr-O stretching vibration [27,28], thus indicating the presence of $\text{NH}_2\text{-UiO-66}$ in the composite material. TAPB-PDA-COF is formed by the condensation reaction of the two organic monomers TAPB and PDA through amino and aldehyde groups. The presence of C=N stretching vibration at 1622 cm^{-1} was observed in the spectrum, thus confirming the successful construction of TAPB-PDA-COF [29]. Finally, the absorption characteristic peak of TAPB-PDA-COF was observed in the composite material, thus indicating the successful compounding of $\text{NH}_2\text{-UiO-66}$ and TAPB-PDA-COF (Fig. 2B).

To further analyze the successfully synthesized $\text{NH}_2\text{-UiO-66@TAPB-PDA-COF}$, the elemental composition and chemical valence of the samples were investigated using XPS. Characteristic peaks of O, N, C, and Zr were observed in the XPS spectrum of $\text{NH}_2\text{-UiO-66@TAPB-PDA-COF}$ (Fig. S1). The XPS spectral characteristic peaks of c1s at 288.8, 286.2, and 284.8 eV confirmed the existence of C=O, C-N, and C-C/C=C bonds [30] (Fig. 2C). The high-resolution Zr 3d spectrum can be decomposed into two peaks of Zr $3d_{5/2}$ and Zr $3d_{3/2}$ of Zr, respectively [31] (Fig. 2D). In the high-resolution XPS spectrum of n1s, the two peaks at 399.1 and 400.3 eV correspond to the two bonds of C=N-C and N-H [32] (Fig. 2E). The high-resolution XPS spectrum of O 1s reveals a peak with a binding energy level of 532.1 eV, attributed to the successful formation of the PDA shell on the surface of the MOF. When the diol group of PDA and the carboxylate group of the organic linker interact with Zr as well, the former Zr-O-C peak emerges [33] (Fig. 2F). The above results further support the successful synthesis of the composite material.

By comparing the specific surface area, the nitrogen adsorption-desorption curve characteristics of $\text{NH}_2\text{-UiO-66}$ and $\text{NH}_2\text{-UiO-66@TAPB-PDA-COF}$ are consistent with the type IV curve, indicating that the material has mesoporous characteristics. And after compounding, the specific surface area of $\text{NH}_2\text{-UiO-66@TAPB-PDA-COF}$ is 2.656 times that of $\text{NH}_2\text{-UiO-66}$ (from $30.52\text{ m}^2\cdot\text{g}^{-1}$ to $81.06\text{ m}^2\cdot\text{g}^{-1}$),

indicating that the compounding of $\text{NH}_2\text{-UiO-66}$ and TAPB-PDA-COF can effectively increase the specific surface area of $\text{NH}_2\text{-UiO-66}$, which is more conducive to the subsequent enrichment of CBZ (Fig. S2A). The thermal stability of $\text{NH}_2\text{-UiO-66}$, TAPB-PDA-COF, and $\text{NH}_2\text{-UiO-66@TAPB-PDA-COF}$ was compared by thermogravimetric analysis. $\text{NH}_2\text{-UiO-66}$ has a 10% mass loss at 198°C , which may come from the loss of moisture and organic matter in the pores. TAPB-PDA-COF has a 10% mass loss at 491°C , while the composite $\text{NH}_2\text{-UiO-66@TAPB-PDA-COF}$ has a 10% mass loss at 321°C , which indicates that the polyimide bond skeleton assisted by the strong C=N covalent bond in TAPB-PDA-COF can produce good chemical stability and make it have strong heat resistance [34]. And TAPB-PDA-COF and $\text{NH}_2\text{-UiO-66@TAPB-PDA-COF}$ showed a sharp decrease in weight at $500\text{--}600^\circ\text{C}$, which may be due to the collapse of the TAPB-PDA-COF structure (Fig. S2B). Therefore, the introduction of TAPB-PDA-COF can effectively improve the thermal stability of $\text{NH}_2\text{-UiO-66}$.

3.3. Optical performance research

$\text{NH}_2\text{-UiO-66}$ shows a strong absorption response in the ultraviolet region, which is due to the presence of benzene rings and amino groups, resulting in the occurrence of $\pi \rightarrow \pi^*$ and $n \rightarrow \pi^*$ transitions [35]. TAPB-PDA-COF has light absorption in the visible region of $400\text{--}500\text{ nm}$. After the material is compounded, the absorption range of $\text{NH}_2\text{-UiO-66@TAPB-PDA-COF}$ is significantly wider than that of $\text{NH}_2\text{-UiO-66}$, and the absorption intensity in the visible region is enhanced (Fig. S3A), further indicating the success of the material compounding. Through fluorescence emission spectrum analysis, $\text{NH}_2\text{-UiO-66}$ shows a strong fluorescence emission at about 428 nm , which can be attributed to the $\pi \rightarrow \pi$ electron transition of the aromatic ring in the 2-aminoterephthalic acid ligand [36]. However, under the same excitation wavelength, TAPB-PDA-COF has no fluorescence response, and the position of the maximum emission wavelength of the composite material is consistent with that of $\text{NH}_2\text{-UiO-66}$. Therefore, the fluorescence emission signal of the composite material comes from $\text{NH}_2\text{-UiO-66}$, and the compound of TAPB-PDA-COF does not affect the position of the maximum emission wavelength of the composite fluorescence (Fig. S3B).

3.4. Feasibility analysis of fluorescent probes

Firstly, the emission performance of $\text{NH}_2\text{-UiO-66@TAPB-PDA-COF}$ was analyzed under different excitation wavelengths. When the excitation wavelength increased from 280 nm to 340 nm, the position of the emission wavelength of $\text{NH}_2\text{-UiO-66@TAPB-PDA-COF}$ did not change accordingly, indicating that the composite material has no dependence on the excitation wavelength and will reduce the interference of autofluorescence. Moreover, when the excitation wavelength was 330 nm, the fluorescent intensity reached the maximum value (Fig. S4A). Therefore, experiments were performed at this excitation wavelength. Then, by adding CBZ to $\text{NH}_2\text{-UiO-66}$ and $\text{NH}_2\text{-UiO-66@TAPB-PDA-COF}$ for analysis, it was found that the fluorescence intensity decreased, indicating that CBZ entered the cavity of $\text{NH}_2\text{-UiO-66}$, resulting in energy transfer between $\text{NH}_2\text{-UiO-66}$ as the donor and CBZ as the receptor. By comparing the ratio of F/F_0 before and after adding CBZ, it was found that the fluorescence response to CBZ was higher after material compounding, indicating that the combination of hydrophobic TAPB-PDA-COF can promote the enrichment of CBZ with lower polarity on the surface of its composite material through the large π conjugated system (Fig. S4B), further improving the detection sensitivity.

3.5. Possible mechanism

Through UV-vis spectral analysis, it is known that carbendazim presents an ultraviolet absorption peak at 282 nm, which may be related to the $\pi \rightarrow \pi^*$ transition of the aromatic ring sp^2 domain existing in carbendazim itself [24] (Fig. 3A). Further measurement of the excitation spectrum and emission spectrum of $\text{NH}_2\text{-UiO-66@TAPB-PDA-COF}$ found that the ultraviolet absorption peak of carbendazim does not overlap with the excitation spectrum and emission spectrum of the fluorescence probe. Therefore, the ability of $\text{NH}_2\text{-UiO-66@TAPB-PDA-COF}$ to be selectively quenched by carbendazim has nothing to do with FRET and IFE. Further, by comparing the FT-IR spectra of $\text{NH}_2\text{-UiO-66@TAPB-PDA-COF}$ before and after the addition of carbendazim, it can be found that the addition of carbendazim does not cause the generation of new functional groups in $\text{NH}_2\text{-UiO-66@TAPB-PDA-COF}$, thereby further excluding the possibility that the fluorescence detection mechanism is SQE [37] (Fig. 3B). Time-resolved transient fluorescence spectroscopy (TR-PL) was used for the analysis. When CBZ was introduced, the $\text{NH}_2\text{-UiO-66@TAPB-PDA-COF}$ fluorescence lifetime underwent a significant dynamic burst ($\tau_{\text{ave}} = 1.527$ ns to $\tau_{\text{ave}} = 0.881$ ns) (Table S1). The decay behaviour is consistent with the third-order dynamics of a typical PET process, which originates from the establishment of an electron transfer channel between the CBZ molecule and $\text{NH}_2\text{-UiO-66}$, and results from the directional migration of the excited state electrons of the donor $\text{NH}_2\text{-UiO-66}$ to the electron-deficient aromatic ring of the acceptor CBZ via interfacial π - π stacking action (Fig. 3C).

To further infer the mechanism of action, XPS analysis of fluorescent

probes before and after the addition of CBZ. The peak of the high-resolution spectrum of N 1s located at 400.3 eV shifted to 401.1 eV, indicating that there may be hydrogen bond interaction between $\text{NH}_2\text{-UiO-66@TAPB-PDA-COF}$ and CBZ [38] (Fig. 4A). Further analysis of the C 1s spectrum showed that after the addition of CBZ, the peak at 288.8 eV shifted to 289.0 eV, which may be caused by π - π interaction (Fig. 4B). Observation via FT-IR reveals the presence of absorption spectral peaks in the range of 1300–1500 cm^{-1} for both carbendazim and the fluorescent probe, indicating the presence of benzene ring structures in both. Since CBZ belongs to the benzimidazole class of compounds, it contains a nitrogen-containing aromatic ring structure and has a strong electron affinity, thus serving as an electron acceptor, prone to forming van der Waals forces and hydrogen bonds [39]. Additionally, $\text{NH}_2\text{-UiO-66@TAPB-PDA-COF}$ possesses a large π conjugated system that can provide electrons, and TAPB-PDA-COF has hydrophobic interaction that can promote the enrichment of substances with lower polarity. Consequently, the fluorescent probe can achieve the selective adsorption of carbendazim through the interaction of its surface groups with CBZ. Combining the above experimental results, it is speculated that carbendazim can interact with the surface groups of $\text{NH}_2\text{-UiO-66@TAPB-PDA-COF}$ through π - π interaction, hydrogen bonding, and hydrophobic interaction, resulting in electron transfer, thereby quenching the fluorescence of $\text{NH}_2\text{-UiO-66@TAPB-PDA-COF}$. Therefore, it is determined that the quenching mechanism of carbendazim is PET [40]. This unique recognition mechanism enables sensitive detection of CBZ.

3.6. Experimental detection condition optimization

To obtain the optimal detection conditions of the fluorescent probe for the target, the pH of the buffer was first explored and analyzed. Different pH values may affect the protonation/deprotonation process on the surface of the composite material, thereby affecting the fluorescence performance during the detection process. In the range of pH 4–9 of the phosphate buffer solution, it can be found that as the pH continues to increase, the fluorescence response of $\text{NH}_2\text{-UiO-66@TAPB-PDA-COF}$ to CBZ detection continues to increase, reaching a maximum at pH 7. With the further increase of pH from 7, the fluorescence response no longer changes significantly. This may be due to the enhanced interaction between the composite material and CBZ during the deprotonation process of the surface groups of $\text{NH}_2\text{-UiO-66@TAPB-PDA-COF}$ under neutral or alkaline conditions, thereby improving the fluorescence response [37]. Therefore, a PBS buffer solution with a pH value of 7 was selected for subsequent experimental exploration (Fig. S5A). Secondly, the effect of different concentrations of fluorescent probes on the detection of CBZ was investigated. It can be found that when the concentration of $\text{NH}_2\text{-UiO-66@TAPB-PDA-COF}$ increases, its fluorescence response to CBZ shows an upward trend. When the concentration reaches 50 $\mu\text{g/mL}$, the fluorescence response remains basically unchanged, and the interaction between the fluorescent probe and CBZ reaches

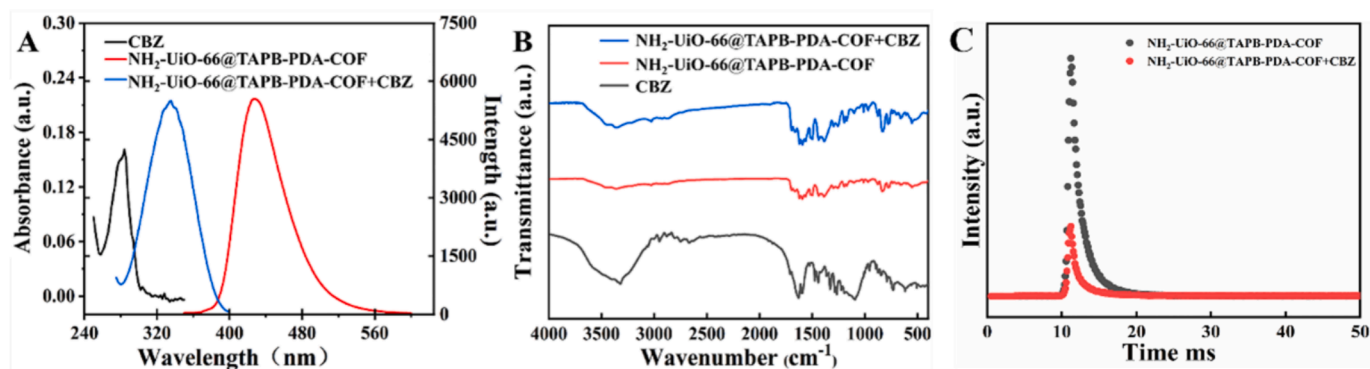


Fig. 3. (A) UV-vis spectra of CBZ, fluorescence excitation spectra and emission spectra of $\text{NH}_2\text{-UiO-66@TAPB-PDA-COF}$; (B) FT-IR spectrum of CBZ, $\text{NH}_2\text{-UiO-66@TAPB-PDA-COF}$ and $\text{NH}_2\text{-UiO-66@TAPB-PDA-COF} + \text{CBZ}$; (C) TR-PL spectra.

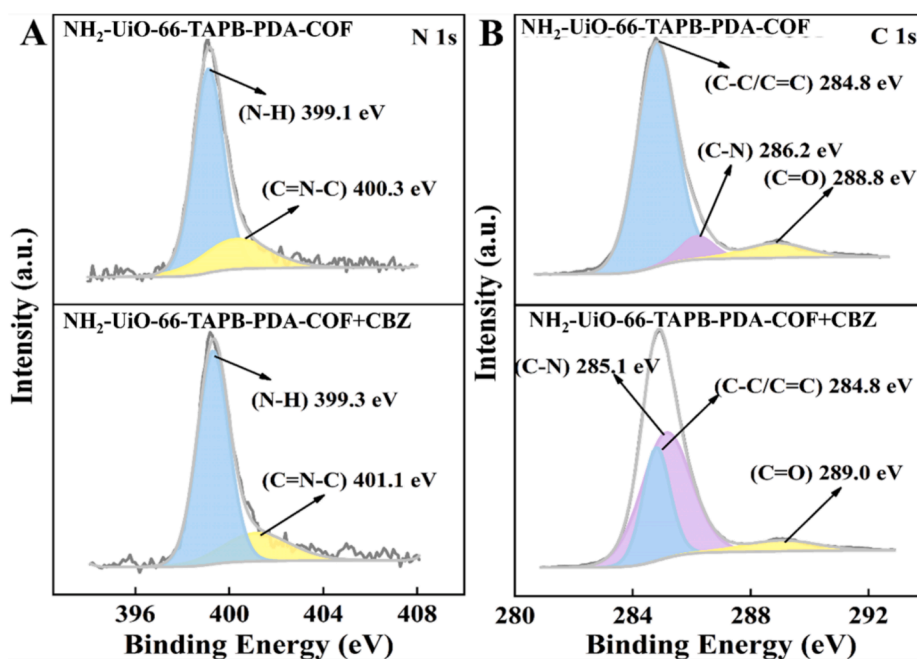


Fig. 4. (A) N 1s and (B) C 1s XPS narrow scan spectra of $\text{NH}_2\text{-UiO-66@TAPB-PDA-COF}$ before and after adding CBZ.

saturation currently (Fig. S5B). Therefore, the concentration of $\text{NH}_2\text{-UiO-66@TAPB-PDA-COF}$ of 50 $\mu\text{g/mL}$ was used in subsequent experiments. Finally, the effect of temperature on the fluorescence response of $\text{NH}_2\text{-UiO-66@TAPB-PDA-COF}$ was investigated. Under the condition of 15–65°C, the detection performance of the fluorescence sensing method hardly changed, and the sensing system has good temperature adaptability (Fig. S5C). Therefore, considering the cost and convenience of rapid detection, 25°C was selected as the subsequent detection temperature.

3.7. Performance analysis of fluorescent probes

The fluorescent probe was used for the actual sample detection and analysis under the optimal conditions. In the range of 1–50.00 $\mu\text{mol/L}$, the fluorescence response intensity of the probe is inversely proportional to the concentration of CBZ and has a good linear relationship (Fig. 5A). The linear regression equation is $y = -0.01740x + 1.019$ ($R^2 = 0.9949$), and the detection limit LOD is 0.1000 $\mu\text{mol/L}$ ($S/N = 3$) (Fig. 5B). Compared with other previously reported methods, the fluorescent probe constructed in this paper has a comparable LOD for the determination of CBZ to other sensing methods. However, the material cost of this fluorescence sensing method is relatively low compared to other

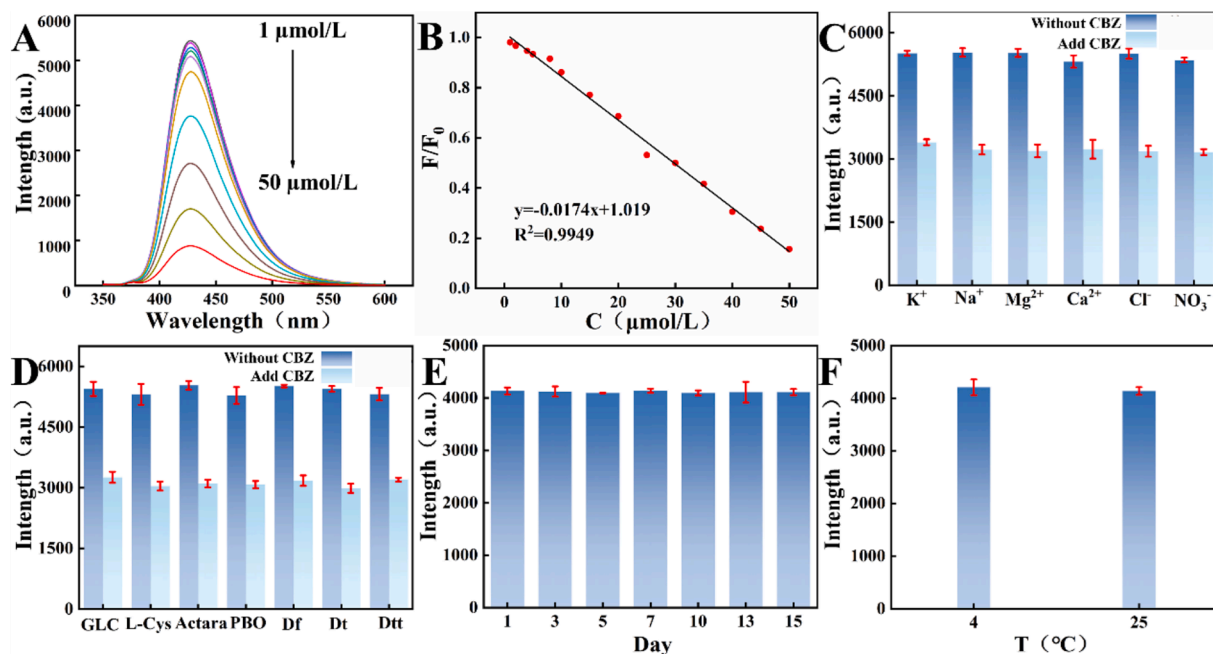


Fig. 5. (A) Fluorescence spectra after gradual addition of CBZ (1–50 $\mu\text{mol/L}$); (B) Linear relationship between CBZ concentration and F/F_0 ; (C–D) Selectivity; (E–F) Specificity.

sensing methods, and the synthesis method is also relatively simple. Moreover, the composite material combines the excellent fluorescence performance of the Zr-based MOFs (NH₂-UiO-66) and the enrichment performance of the hydrophobic TAPB-PDA-COF with a large π -conjugated system for the less polar CBZ. Under the synergistic effect of the two materials, the Zr-based MOFs and the hydrophobic COF, the composite NH₂-UiO-66@TAPB-PDA-COF has the potential for rapid detection of CBZ (Table S2).

Selectivity and stability are also crucial for evaluating the detection ability of fluorescent sensors. Firstly, the selectivity was investigated by choosing cations and anions (K⁺, Na⁺, Mg²⁺, Ca²⁺, Cl⁻, and NO³⁻), functional substances (glucose and L-cysteine), and pesticides (thiamethoxam, imidacloprid, dinotefuran, dimethoate, and trichlorfon) as interfering substances, whose concentrations were five times that of carbendazim. The addition of interfering substances did not cause a response from the fluorescent probe. However, when CBZ was added, fluorescence quenching occurred, indicating that the constructed fluorescent probe has good selectivity for CBZ (Fig. 5C–D). Finally, after the fluorescent probe was reused continuously for 15 days and at different storage temperatures simultaneously, the fluorescence response of the fluorescence probe basically did not change, and the RSD was only 1.9%, indicating that the fluorescent probe has good stability (Fig. 5E–F).

3.8. Real sample analysis

The determination of CBZ content in real samples of fruits and vegetables (apples, oranges, cucumbers, lettuce), water samples (tap water, lake water) and soil by the fluorescent probe of NH₂-UiO-66@TAPB-PDA-COF was carried out to explore its feasibility and applicability in practical applications. Firstly, these fruits, vegetables and water samples were pretreated, and CBZ with a concentration of 5 μ mol/L and 10 μ mol/L was added to maintain the concentration of CBZ in the actual samples for fluorescence testing. The recovery range of the samples tested was from 94.21% to 107.80%. The relative standard deviation (RSD) determined was less than 7.09%. In addition, HPLC was used to verify the content of CBZ in actual samples, with a recovery rate of 95.11–108.13% and an RSD less than 5.98%, indicating that there is no detection difference between the prepared sensor and HPLC. The results indicate that the constructed sensing platform possesses excellent performance in detecting CBZ and can be applied in practical scenarios (Table S3).

4. Conclusions

To sum up, a novel fluorescent probe with enrichment and fluorescence characteristics was prepared by coating the surface of NH₂-UiO-66 with TAPB-PDA-COF through the interface growth method, which can efficiently and sensitively detect CBZ. The fluorescence probe and CBZ produce an anti-pet effect through π - π interaction, hydrogen bonding, and hydrophobic interaction, thereby quenching the fluorescence, so CBZ can be detected sensitively through the fluorescence signal. This fluorescent probe has the advantages of fast response speed, low detection limit, and wide linear range. This work provides a theoretical reference for the combination of MOFs and COFs to construct fluorescent probes and provides a potential strategy for the rapid detection of pesticides.

CRedit authorship contribution statement

Lei Sun: Writing – original draft, Visualization, Methodology, Investigation, Formal analysis. **Rui Zhou:** Validation, Methodology, Investigation, Formal analysis. **Ru-Chao Wang:** Investigation, Formal analysis. **Yue-Hong Pang:** Methodology, Investigation, Formal analysis. **Xiao-Fang Shen:** Writing – review & editing, Resources, Project administration, Funding acquisition.

Declaration of competing interest

The authors declare that they have no known competing financial interests or personal relationships that could have appeared to influence the work reported in this paper.

Acknowledgments

This work was supported by the National Key Research and Development Program of China (2022YFF1100803). Xinjiang Uygur Autonomous Region Intellectual Aid Xinjiang Innovation and Expansion Talent Projects.

Appendix A. Supplementary data

Supplementary data to this article can be found online at <https://doi.org/10.1016/j.microc.2025.113464>.

Data availability

Data will be made available on request.

References

- [1] J. Shi, M. Zhao, K. Li, Y. Zhao, W. Li, Y. Peng, J. Zheng, Metabolic activation and cytotoxicity of fungicide carbendazim mediated by CYP1A2, *J. Agric. Food Chem.* 70 (2022) 4092–4101, <https://doi.org/10.1021/acs.jafc.1c08144>.
- [2] S. Velmurugan, P. Traiwatcharanon, P.K. Jiwanti, S.-H. Cheng, C. Wongchoosuk, Highly selective carbendazim fungicide sensing performance of nitrogen-doped carbon quantum dots encapsulated aminated-UiO-66 zirconium metal-organic framework electrocatalyst, *Electrochim. Acta.* 479 (2024) 143911–143922, <https://doi.org/10.1016/j.electacta.2024.143911>.
- [3] K. Liu, X. Pan, Y. Han, F. Tang, Y. Yu, Estimating the toxicity of the weak base carbendazim to the earthworm (*Eisenia fetida*) using in situ pore water concentrations in different soils, *Sci. Total Environ.* 438 (2012) 26–32, <https://doi.org/10.1016/j.scitotenv.2012.08.008>.
- [4] D. Ilager, N.P. Shetti, Y. Foucaud, M. Badawi, T.M. Aminabhavi, Graphene/g-carbon nitride (GO/g-C₃N₄) nanohybrids as a sensor material for the detection of methyl parathion and carbendazim, *Chemosphere* 292 (2022) 133450–133464, <https://doi.org/10.1016/j.chemosphere.2021.133450>.
- [5] G.L. Scheel, C.R. Teixeira Tarley, Simultaneous microextraction of carbendazim, fipronil and picoxystrobin in naturally and artificial occurring water bodies by water-induced supramolecular solvent and determination by HPLC-DAD, *J. Mol. Liq.* 297 (2020) 111897–111906, <https://doi.org/10.1016/j.molliq.2019.111897>.
- [6] Y. Zhai, T. Xuan, Y. Wu, X. Guo, Y. Ying, Y. Wen, H. Yang, Metal-organic-frameworks-enforced surface enhanced Raman scattering chip for elevating detection sensitivity of carbendazim in seawater, *Sensor. Actuat. B-Chem.* 326 (2021) 128852–128858, <https://doi.org/10.1016/j.snb.2020.128852>.
- [7] A.M. Oliveira, H.C. Loureiro, F.F.S. de Jesus, D.P. de Jesus, Electromembrane extraction and preconcentration of carbendazim and thiabendazole in water samples before capillary electrophoresis analysis, *J. Sep. Sci.* 40 (2017) 1532–1539, <https://doi.org/10.1002/jssc.201601305>.
- [8] W. Jin, L. Ruiyi, L. Nana, S. Xiulan, Z. Haiyan, W. Guangli, L. Zaijun, Electrochemical detection of carbendazim with mulberry fruit-like gold nanocrystal/multiple graphene aerogel and DNA cycle amplification, *Microchim. Acta* 188 (2021) 214122–214134, <https://doi.org/10.1007/s00604-021-04886-y>.
- [9] L. Wang, W. Ahmad, J. Wu, X. Wang, Q. Chen, Q. Ouyang, Selective detection of carbendazim using an upconversion fluorescence sensor modified by biomimetic molecularly imprinted polymers, *Spectrochim. Acta A* 284 (2023) 121457–121467, <https://doi.org/10.1016/j.saa.2022.121457>.
- [10] X. Chen, G. Li, X. Yue, C. Peng, J. Wang, Ratiometric fluorescent detection of carbendazim in foods based on metallic nanoclusters self-assembled nanocomplex, *Food Chem.* 424 (2023) 136478–136484, <https://doi.org/10.1016/j.foodchem.2023.136478>.
- [11] L. Chen, D. Litu, J. Peng, Q. Du, H. He, Ratiometric fluorescence sensing of metal-organic frameworks: Tactics and perspectives, *Coord. Chem. Rev.* 404 (2020) 213113–213140, <https://doi.org/10.1016/j.ccr.2019.213113>.
- [12] T. Leelasree, S. Goel, H. Aggarwal, MOF-Based dual sensor for the electrochemical and fluorescence detection of nicotine, *ACS Appl. Nano Mater.* 5 (2022) 16753–16759, <https://doi.org/10.1021/acsnano.2c03751>.
- [13] C. Mao, R.A. Kudla, F. Zuo, X. Zhao, L.J. Mueller, X. Bu, P. Feng, Anion stripping as a general method to create cationic porous framework with mobile anions, *J. Am. Chem. Soc.* 136 (2014) 7579–7582, <https://doi.org/10.1021/ja5030723>.
- [14] H. Kim, H. Kim, K. Kim, E. Lee, Structural control of metal-organic framework bearing n-heterocyclic imidazolium cation and generation of highly stable porous structure, *Inorg. Chem.* 58 (2019) 6619–6627, <https://doi.org/10.1021/acs.inorgchem.8b03173>.
- [15] Y. Zhang, M. Sun, M. Peng, E. Du, X. Xu, C.-C. Wang, The fabrication strategies and enhanced performances of metal-organic frameworks and carbon dots composites:

- State of the art review, *Chin. Chem. Lett.* 34 (2023) 107478–107495, <https://doi.org/10.1016/j.ccllet.2022.04.076>.
- [16] Y. Liu, X.-Y. Xie, C. Cheng, Z.-S. Shao, H.-S. Wang, Strategies to fabricate metal–organic framework (MOF)-based luminescent sensing platforms, *J. Mater. Chem. C* 7 (2019) 10743–10763, <https://doi.org/10.1039/c9tc03208h>.
- [17] C. Guo, F. Duan, S. Zhang, L. He, M. Wang, J. Chen, J. Zhang, Q. Jia, Z. Zhang, M. Du, Heterostructured hybrids of metal–organic frameworks (MOFs) and covalent–organic frameworks (COFs), *J. Mater. Chem. A* 10 (2022) 475–507, <https://doi.org/10.1039/d1ta06006f>.
- [18] R. Xue, H. Guo, W. Yang, S.-L. Huang, G.-Y. Yang, Cooperation between covalent organic frameworks (COFs) and metal organic frameworks (MOFs): application of COFs-MOFs hybrids, *Adv. Compos. Hybrid Ma.* 5 (2022) 1595–1611, <https://doi.org/10.1007/s42114-022-00432-3>.
- [19] W. Li, Z. Hu, J. Meng, X. Zhang, W. Gao, M. Chen, J. Wang, Zn-based metal organic framework-covalent organic framework composites for trace lead extraction and fluorescence detection of TNP, *J. Hazard. Mater.* 411 (2021) 125021–125032, <https://doi.org/10.1016/j.jhazmat.2020.125021>.
- [20] J. Wan, W. Shi, Y. Li, Y. Yu, X. Wu, Z. Li, S.-Y. Lee, K.H. Lee, Excellent crystallinity and stability covalent–organic frameworks with high emission and anions sensing, *Macromol. Rapid Comm.* 43 (2022) 2200393–2200402, <https://doi.org/10.1002/marc.202200393>.
- [21] D. Feng, T. Zhang, T. Zhong, C. Zhang, Y. Tian, G. Wang, Coumarin-embedded MOF UiO-66 as a selective and sensitive fluorescent sensor for the recognition and detection of Fe³⁺ ions, *J. Mater. Chem. C* 9 (2021) 16978–16984, <https://doi.org/10.1039/d1tc03516a>.
- [22] L. Chen, Y. He, Z. Lei, C. Gao, Q. Xie, P. Tong, Z. Lin, Preparation of core-shell structured magnetic covalent organic framework nanocomposites for magnetic solid-phase extraction of bisphenols from human serum sample, *Talanta* 181 (2018) 296–304, <https://doi.org/10.1016/j.talanta.2018.01.036>.
- [23] L. Zhong, J. Zhong, Z. Gu, X. Zhang, Q. Zhou, H. Zhai, Synthesis of composite materials combining magnetic metal-organic frameworks and conjugated organic frameworks for selective extraction of carbendazim and thiabendazole residues from Chinese herbal medicine samples, *J. Chromatogr. A* 1712 (2023) 464474–464486, <https://doi.org/10.1016/j.chroma.2023.464474>.
- [24] Y. Han, X. He, W. Yang, X. Luo, Y. Yu, W. Tang, T. Yue, Z. Li, Ratiometric fluorescent sensing carbendazim in fruits and vegetables via its innate fluorescence coupling with UiO-67, *Food Chem.* 345 (2021) 128839–128848, <https://doi.org/10.1016/j.foodchem.2020.128839>.
- [25] Q. Du, P. Wu, Y. Sun, J. Zhang, H. He, Selective photodegradation of tetracycline by molecularly imprinted ZnO@NH₂-UiO-66 composites, *Chem. Eng. J.* 390 (2020) 124614–124625, <https://doi.org/10.1016/j.cej.2020.124614>.
- [26] S. Jing, H. Wang, A. Wang, R. Cheng, H. Liang, F. Chen, A. Brouzougou, P. Tsiakaras, Surface plasmon resonance Bismuth-modified NH₂-UiO-66 with enhanced photocatalytic tetracycline degradation performance, *J. Colloid Interface Sci.* 655 (2024) 120–132, <https://doi.org/10.1016/j.jcis.2023.10.149>.
- [27] W. Hu, F. Pei, S. Feng, B. Du, B. Liu, X. Mu, Z. Tong, A smartphone-assisted dual-response imprinted fluorescence sensor based on UiO-66 and quantum dots for detecting bovine hemoglobin, *Microchem. J.* 191 (2023) 108825–108833, <https://doi.org/10.1016/j.microc.2023.108825>.
- [28] C. Yu, J. Zhang, X. Luo, J. Zhang, Metal organic framework/covalent organic framework composite for solid-phase microextraction of polycyclic aromatic hydrocarbons in milk samples, *Microchem. J.* 187 (2023) 108388–108398, <https://doi.org/10.1016/j.microc.2023.108388>.
- [29] S. Lu, S. Wang, P. Wu, D. Wang, J. Yi, L. Li, P. Ding, H. Pan, A composite prepared from covalent organic framework and gold nanoparticles for the electrochemical determination of enrofloxacin, *Adv. Powder Technol.* 32 (2021) 2106–2115, <https://doi.org/10.1016/j.apt.2021.04.025>.
- [30] P. Jia, K. Yang, J. Hou, Y. Cao, X. Wang, L. Wang, Ingenious dual-emitting Ru@UiO-66-NH₂ composite as ratiometric fluorescence sensor for detection of mercury in aqueous, *J. Hazard. Mater.* 408 (2021) 124469–124477, <https://doi.org/10.1016/j.jhazmat.2020.124469>.
- [31] P. Huo, Z. Li, C. Gong, R. Yao, C. Fan, Z. Chen, S. Pu, Silver nanoparticles combined with amino-functionalized UiO-66 for sensitive detection of glutathione, *Spectrochim. Acta A* 267 (2022) 120617–120625, <https://doi.org/10.1016/j.saa.2021.120617>.
- [32] K. Yi, X. Zhang, L. Zhang, Smartphone-based ratiometric fluorescent definable system for phosphate by merged metal–organic frameworks, *Sci. Total Environ.* 772 (2021) 144952–144961, <https://doi.org/10.1016/j.scitotenv.2021.144952>.
- [33] N. Celebi, M.Y. Aydin, F. Soysal, N. Yıldız, K. Salimi, Core/shell PDA@UiO-66 metal–organic framework nanoparticles for efficient visible-light photodegradation of organic dyes, *ACS Appl. Nano Mater.* 3 (2020) 11543–11554, <https://doi.org/10.1021/acsam.0c02636>.
- [34] J. Wang, L. Si, Q. Wei, X. Hong, L. Lin, X. Li, J. Chen, P. Wen, Y. Cai, An imine-linked covalent organic framework as the host material for sulfur loading in lithium–sulfur batteries, *J. Energy Chem.* 28 (2019) 54–60, <https://doi.org/10.1016/j.jechem.2017.10.021>.
- [35] C. Li, X. Xu, J. Xing, F. Wang, Y. Shi, X. Zhao, J. Liu, Y. Yang, Z. Zhao, A fluorescent dual-emissions UiO-66-NH₂@TpTt-COF core-shell composite for sensitive and optosmart sensing of tetracycline, *Appl. Surf. Sci.* 616 (2023) 156455–156464, <https://doi.org/10.1016/j.apsusc.2023.156455>.
- [36] P. Wu, Q. Du, L. Chen, M. Yang, Y. Sun, H. Zhi, P. Dramou, H. He, Fluorescence determination of quercetin in food samples using polyhedron-shaped MOF@MOF (NUZ-8) based on NH₂-UiO-66 and ZIF-8, *Microchim. Acta.* 188 (1) (2021) 118–127, <https://doi.org/10.1007/s00604-020-04664-2>.
- [37] H. Guo, R. Yang, D. Lei, X. Ma, D. Zhang, P. Li, J. Wang, L. Zhou, W. Kong, Red-emissive carbon dots based fluorescent and smartphone-integrated paper sensors for sensitive detection of carbendazim, *Microchem. J.* 190 (2023) 108586–108594, <https://doi.org/10.1016/j.microc.2023.108586>.
- [38] H. Guo, Y. Li, Y. Li, X. He, L. Chen, Y. Zhang, Construction of stable magnetic vinylene-linked covalent organic frameworks for efficient extraction of benzimidazole fungicides, *ACS Appl. Mater.* (2023) 14777–14787, <https://doi.org/10.1021/acsami.2c22386>.
- [39] Y. Han, H. Wang, Y. Yu, W. Yang, F. Shang, Z. Li, Impact on ratiometric fluorescence of carbon dots hybridizing with lanthanide in determination of residual Carbendazim in food, *Appl. Surf. Sci.* 606 (2022) 154700–154710, <https://doi.org/10.1016/j.apsusc.2022.154700>.
- [40] Y. Qiang, W. Yang, X. Zhang, X. Luo, W. Tang, T. Yue, Z. Li, UiO-67 decorated on porous carbon derived from Ce-MOF for the enrichment and fluorescence determination of glyphosate, *Microchim. Acta* 189 (3) (2022) 189–200, <https://doi.org/10.1007/s00604-022-05236-2>.